Molecular Imaging
Volume 15 : 1-15
© The Author(s) 2016
Reprints and permission:
sagepub.com/journalsPermissions.nav
DOI: 10.1177/1536012115624920
mix.sagepub.com
SAGE

Comparison of New Tau PET-Tracer Candidates With [^{18}F]T808 and [^{18}F]T807

Lieven Declercq, Pharmacist[1], Sofie Celen, PhD[1], Joan Lecina, PhD[1], Muneer Ahamed, PhD[1], Thomas Tousseyn, Prof, MD, PhD[2], Diederik Moechars, PhD[3], Jesus Alcazar, PhD[4], Manuela Ariza, PhD[4], Katleen Fierens, PhD[4], Astrid Bottelbergs, PhD[3], Jonas Mariën, PhD[3], Rik Vandenberghe, Prof, MD, PhD[5], Ignacio Jose Andres, PhD[4], Koen Van Laere, Prof, MD, PhD[6], Alfons Verbruggen, Prof, PhD[1], and Guy Bormans, Prof, PhD[1]

Abstract

Early clinical results of two tau tracers, [^{18}F]T808 and [^{18}F]T807, have recently been reported. In the present study, the biodistribution, radiometabolite quantification, and competition-binding studies were performed in order to acquire comparative preclinical data as well as to establish the value of T808 and T807 as benchmark compounds for assessment of binding affinities of eight new/other tau tracers. Biodistribution studies in mice showed high brain uptake and fast washout. *In vivo* radiometabolite analysis using high-performance liquid chromatography showed the presence of polar radiometabolites in plasma and brain. No specific binding of [^{18}F]T808 was found in transgenic mice expressing mutant human P301L tau. In semiquantitative autoradiography studies on human Alzheimer disease slices, we observed more than 50% tau selective blocking of [^{18}F]T808 in the presence of 1 μmol/L of the novel ligands. This study provides a straightforward comparison of the binding affinity and selectivity for tau of the reported radiolabeled tracers BF-158, BF-170, THK5105, lansoprazole, astemizole, and novel tau positron emission tomography ligands against T807 and T808. Therefore, these data are helpful to identify structural requirements for selective interaction with tau and to compare the performance of new highly selective and specific radiolabeled tau tracers.

Keywords

molecular imaging of neurodegenerative diseases, Alzheimer, biomarker, PET imaging

Introduction

In spite of extensive knowledge about epidemiology, histopathological features, and genetics of Alzheimer disease (AD), only symptomatic treatment is available at this moment.[1] Therefore, there is a great need for an efficient treatment that can be initiated in an early phase of the disease. Definite diagnosis can still only be made postmortem on the basis of two pathological hallmarks: senile plaques (SP) and neurofibrillary tangles (NFTs).[2] Both SP and NFTs have been targeted by positron emission tomography (PET) ligands that can serve as diagnostic biomarkers, as this is a sensitive *in vivo* method to visualize and quantify AD-specific pathological changes in the living brain.[3]

Much effort has been invested in the development of PET tracers that specifically bind to amyloid beta sheets (Aβ). While a negative scan substantially limits the chance for

[1] Laboratory for Radiopharmacy, Department of Pharmaceutical and Pharmacological Sciences, KU Leuven, Leuven, Belgium
[2] Translational Cell and Tissue Research, Department of Imaging and Pathology, KU Leuven, Leuven, Belgium
[3] Janssen Research and Development, Neuroscience Discovery Biology, a division of Janssen Pharmaceutica NV, Beerse, Belgium
[4] Janssen Research and Development, Discovery Sciences, a division of Janssen-Cilag NV, Toledo, Belgium
[5] Laboratory for Cognitive Neurology, Department of Neurosciences, KU Leuven, Leuven, Belgium
[6] Nuclear Medicine & Molecular Imaging, Department of Imaging and Pathology, KU Leuven, Leuven, Belgium

Submitted: 17/09/2015. Revised: 23/10/2015. Accepted: 15/11/2015.

Corresponding Author:
Guy Bormans, KU Leuven, Leuven, Belgium.
Email: guy.bormans@pharm.kuleuven.be

development of AD and greatly influences clinic decision making, a positive amyloid PET scan is, by itself, not sufficient for a positive diagnosis for AD.[4] In contrast, even at late stages of AD, the burden of NFTs is closely related to the clinical symptoms of AD.[5-7] This likely implicates that a PET tracer that selectively targets tau aggregates could be a more relevant biomarker for AD conversion and for neurodegenerative tauopathies.[8]

Several aspects make the development of tau imaging agents challenging. Through alternative splicing of the microtubule-associated protein tau gene, six isoforms of tau are expressed in the adult human central nervous system, giving rise to two sets of isoforms: those with three (3R) and those with four (4R) microtubule-binding domains, the latter one being more efficient in stabilizing microtubules. Normally, there is an equal ratio of both isoforms, but under pathological circumstances, several tauopathies express different isoform ratios with diverse morphologies. Due to these structural differences, it may be difficult to develop a tau-specific tracer, with similar affinity for every phenotype.[7] Furthermore, tau is subjected to many posttranslational modifications, which may result in conformational changes in the aggregates, potentially leading to different binding affinities of tau ligands.[9] Additionally, tau tracers need to be highly selective, as in AD, tau aggregates are coexistent with Aβ deposits but occur in concentrations ~5 to 20 times lower than Aβ aggregates.[7] Despite many hurdles, several tau PET imaging agents have already been reported.[8,10-14] For six of those agents, 2-(1-(6-[(2-[^{18}F]fluoroethyl)(methyl)amino]-2-naphtyl)ethylidene) malononitrile, [^{18}F]T808 (also known as [^{18}F]AV-1451), [^{18}F]T807 (also known as [^{18}F]AV-680), [^{18}F]THK523, [^{18}F]THK5105 (Tohoku, of the Tohoku University in Japan), [^{18}F]THK5117, and [^{11}C]2-((1*E*, 3*E*)-4-(6-((^{11}C-methylamino)pyridin-3-yl)buta-1,3-dienyl)benzo[*d*]thiazol-6-ol, evaluation in humans has been reported.[15,16]

[^{18}F]FDDNP, the oldest PET tracer in this series, was first identified as having affinity for Aβ and NFTs. High retention was found in brain of patients with AD and in other tauopathies, but its low Aβ/tau selectivity, relatively low affinity for tau, and small dynamic range of signal limit its use as tau PET tracer.[16,17]

[^{18}F]T808 and [^{18}F]T807 showed reasonable affinity (K_D, respectively 22 and 15 nmol/L) and specificity values (respectively 27- and 25-fold higher binding affinity for NFTs over Aβ) in autoradiography K_D-determination studies on human AD brain tissue sections.[8,11] Early clinical evaluation of both imaging agents seems to confirm preclinical findings.[18,19] With favorable pharmacokinetics and a binding pattern consistent with the Braak staging, they are currently among the most promising PET candidates for tau imaging.[15,20] Substantial defluorination has however been observed with [^{18}F]T808, and no full kinetic modeling of the tracers has been reported yet.[16,19]

Comparable *in vitro* binding assay studies have been performed by other groups with radiolabeled arylquinoline derivatives THK-523, THK-5105, and THK-5117 and recently also with THK-5351.[16] Although [^{18}F]THK-523 showed high affinity and specificity for tau fibrils *in vitro*,[15] unfavorable pharmacokinetics and high white matter binding pushed the development of the new 2-arylquinoline derivatives [^{18}F]THK-5105 and [^{18}F]THK-5117, with higher affinity and lower white matter binding.[13,20]

Compared to these five fluorine-18-labeled compounds, the carbon 11-labeled compound PBB3 is so far the only one published showing high affinity for tau in AD as well as non-AD tauopathies, implying that it may detect multiple tau isoforms.[15] However, the tracer shows rapid metabolism and a challenging radiosynthesis because of its sensitivity to photoisomerization.

In order to obtain comparative preclinical data for [^{18}F]T808 and [^{18}F]T807, we have performed biodistribution, radiometabolite, and autoradiography studies, properties that determine the potential of new PET tracers, as no (comparable) data of these experiments are available in the literature. These properties were also compared for a number of other existing tau tracers and newly designed radioligands in semiquantitative autoradiography studies and competition binding assays, since the aim of this research was to identify structural moieties needed for selective interaction with NFTs and to provide a straightforward comparison of the currently reported tau tracers.

Materials and Methods

General

The precursor and authentic reference material for [^{18}F]T807 and [^{18}F]T808 and the nonradioactive reference material for [^{18}F]THK-5105 were synthesized according to the published procedures.[21,22] All other chemicals and reagents were purchased from commercial sources and used without further purification. The TLC plates (Macherey-Nagel, Düren, Germany) were developed using mixtures of ethyl acetate and heptane or dichloromethane and methanol as mobile phase. Automated flash column chromatography was performed using silica cartridges (GraceResolv 12 g, Grace, Deerfield, Illinois) on a Reveleris X2 flash system (Grace) equipped with an evaporative light-scattering detector and ultraviolet (UV) detector at 254 nm. ^{1}H nuclear magnetic resonance (NMR) spectra were recorded on a Bruker Avance II spectrometer (400 MHz, 5 mm probe; Fällanden, Switzerland) using deuterated methanol (MeOD-*d4*) or deuterated dimethyl sulfoxide (DMSO-*d6*) as indicated. Chemical shifts are reported in parts per million downfield from tetramethylsilane ($\delta = 0$). Coupling constants are reported in hertz (Hz). Splitting patterns are defined by s (singlet), d (doublet), dd (double doublet), dt (double triplet), t (triplet), q (quartet), or m (multiplet). Exact mass measurements were performed on an ultra-high resolution time-of-flight mass spectrometer (maXis impact LC/MS, Bruker, Bremen, Germany) equipped with an orthogonal electrospray ionization (ESI) interface. Acquisition and processing of data were conducted using HyStar and Compass DataAnalysis (version 3.2; Bruker), respectively. Calculated monoisotopic

mass values were obtained using MarvinSketch (version 6.1.0; ChemAxon http://www.chemaxon.com). High-performance liquid chromatography (HPLC) analysis was performed on a LaChrom Elite HPLC system (Hitachi, Darmstadt, Germany) connected to a UV detector set at 254 nm. For analysis of radiolabeled compounds, the HPLC eluate, after passing through the UV detector, was led over a 3-inch sodium iodide activated with thallium NaI(Tl) scintillation detector connected to a single-channel analyzer (GABI box; Raytest, Straubenhardt, Germany). Data were acquired and analyzed using GINA Star (Raytest) data acquisition systems. Quantification of radioactivity in samples of biodistribution and radiometabolite studies was performed using an automated γ-counter equipped with a 3-inch NaI(Tl) well crystal coupled to a multichannel analyzer, mounted in a sample changer (Wallac 2480 Wizard 3q; Wallac, Turku, Finland). The values are corrected for background radiation, physical decay, and counter dead time. Alzheimer disease slices of 10 µm thick from the visual cortex of a 68-year-old woman in the latest Braak stage (V-VI) were provided by University Hospitals Leuven (Neurology Department, Leuven, Belgium) after approval from the local ethics committee. Animals were housed in individually ventilated cages in a thermoregulated (~22°C), humidity-controlled facility under a 12-hour–12-hour light–dark cycle, with access to food and water ad libitum. All animal experiments were conducted according to the Belgian code of practice for the care and the use of animals, after approval from the university animal ethics committee.

Chemistry

2-(4-Nitrophenyl)benzo[d]thiazole (TAU1). Compound was synthesized according to a described procedure.[23] Liquid chromatography-high resolution mass spectrometry (LC-HRMS) (ESI) calculated for $C_{13}H_9FNS$ $[MH]^+$ 230.0434, measured 230.0441; ^{1}H NMR (400 MHz, MeOD-*d4*) δ 7.29 (t, 2H, J = 8.7, Ar), 7.44 (t, 2H, J = 7.8, Ar), 7.54 (t, 2H, J = 7.8, Ar), 8.01 (dd, J = 7.9 and 4.0 and 2.0, 2H, Ar), 8.14 (dd, J = 8.6 and 5.5, 2H, Ar).

Methyl 2-(4-nitrophenyl)benzo[d]thiazole-6-carboxylate (TAU2). The compound was synthesized according to a described procedure.[24] LC-HRMS (ESI) calculated for $C_{15}H_{11}N_2O_4S$ $[MH]^+$ 315.0434, measured 315.0454; ^{1}H NMR (400 MHz, DMSO-*d6*) δ 2.34 (s, 3H, OCH_3), 7.39 (dd, J = 8.8 and 2.0, 1H, Ar), 8.07 (d, J = 2.0, 1H, Ar), 8.17 (d, J = 8.8, 1H, Ar), 8.33 to 8.45 (m, 4H, Ar).

2-[4-(4-Fluorophenyl)phenyl]-1,3-benzothiazole (TAU3). The compound was synthesized according to T807's patent application[21] using 4-(benzo[d]thiazol-2-yl)phenylboronic acid and 1-bromo-4-fluorobenzene as starting materials (Figure 1). LC-HRMS (ESI) calculated for $C_{19}H_{13}FNS$ $[MH]^+$ 306.0747, measured 306.0762; ^{1}H NMR (400 MHz, DMSO-*d6*) δ 7.35 (t, J = 8.8, 2H, Ar), 7.48 (t, J = 7.7, 1H, Ar), 7.57 (t, J = 7.7, 1H, Ar), 7.65 to 7.76 (m, 1H, Ar), 7.79 to 7.97 (m, 3H, Ar), 8.09 (d, J = 8.0, 1H, Ar), and 8.14 to 8.25 (m, 3H, Ar).

1-Benzylidene-2-(4-(4-methoxyphenyl)thiazol-2-yl)hydrazine (TAU4). The compound was synthesized according to a described procedure.[25] LC-HRMS (ESI) calculated for $C_{17}H_{16}N_3OS$ $[MH]^+$ 310.1009, measured 310.1017; ^{1}H NMR (400 MHz, DMSO-*d6*) δ 3.78 (s, 3H, OCH_3), 6.96 (d, J = 8.8, 2H, Ar), 7.11 (s, 1H, Phenyl-CH), 7.34 to 7.47 (m, 3H, Ar), 7.64 (d, J = 7.2, 2H, Ar), 7.77 (d, J = 8.8, 2H, Ar), 8.03 (s, 1H, Ar).

2-(4-(4-Methoxyphenyl)thiazol-2-yl)-1-((pyridin-2-yl)methylene)hydrazine (TAU5). The compound was synthesized according to a described procedure.[25] LC-HRMS (ESI) calculated for $C_{16}H_{15}N_4OS$ $[MH]^+$ 311.0961, measured 311.0967; ^{1}H NMR (400 MHz, DMSO-*d6*) δ 3.78 (s, 3H, OCH_3), 6.97 (d, J = 8.6, 2H, Ar), 7.20 (s, 1H, Phenyl-CH), 7.31 to 7.42 (m, 1H, Ar), 7.74 to 7.90 (m, 4H, Ar), 8.05 (s, 1H, Ar), 8.87 (d, J = 4.7, 1H, Ar).

2-Methoxy-5-{5H-pyrido[4,3-b]indol-7-yl}pyridine (TAU6). The compound was synthesized according to T807's patent application[21] using 3-bromo-4-nitropyridine and 4-bromophenylboronic acid as starting materials in the first step and 2-methoxypyridine-5-boronic acid for the second step (Figure 1). LC-HRMS (ESI) calculated for $C_{17}H_{14}N_3O$ $[MH]^+$ 276.1131, measured 276.1153; ^{1}H NMR (400 MHz, DMSO-*d6*) δ 3.90 (s, 3H, OCH_3), 6.93 (d, J = 8.6, 1H, Ar), 7.46 (d, J = 5.6, 1H, Ar), 7.54 (d, J = 8.1, 1H, Ar), 7.75 (s, 1H, Ar), 8.06 to 8.15 (m, 1H, Ar), 8.28 (d, J = 8.1, 1H, Ar), 8.37 to 8.46 (m, 1H, Ar), 8.56 (s, 1H, Ar), 9.33 (s, 1H, Ar).

7-(4-Methoxyphenyl)-5H-pyrido[4,3-b]indole (TAU7). The compound was synthesized according to T807's patent application[21] using 3-bromo-4-nitropyridine and 4-bromophenylboronic acid as starting material in the first step and 4-methoxyphenylboronic acid for the second step (Figure 1). LC-HRMS (ESI) calculated for $C_{18}H_{15}N_2O$ $[MH]^+$ 275.1179, measured 275.1196; ^{1}H NMR (400 MHz, DMSO-*d6*) δ 3.85 (s, 3H, OCH_3), 7.03 (d, J = 8.2, 2H, Ar), 7.48 to 7.58 (m, 2H, Ar), 7.65 (d, J = 8.2, 2H, Ar), 7.71 (s, 1H, Ar), 8.21 (d, J = 8.2, 1H, Ar), 8.37 (d, J = 5.9, 1H, Ar), 9.23 (s, 1H, Ar).

Methyl 5-{5H-pyrido[4,3-b]indol-7-yl}pyridine-2-carboxylate (TAU8). The ompound was synthesized according to T807's patent application[21] using 3-bromo-4-nitropyridine and 4-bromophenylboronic acid as starting materials in the first step and 4-methoxycarbonylphenylboronic acid for the second step (Figure 1). LC-HRMS (ESI) calculated for $C_{18}H_{14}N_3O_2$ $[MH]^+$ 304.1080, measured 304.1088; ^{1}H NMR (400 MHz, DMSO-*d6*) δ 3.92 (s, 3H, $COOCH_3$), 7.40 – 7.14 (m, 1H, Ar), 7.52 (t, J = 8.5, 1H, Ar), 7.72 (dd, J = 8.2 and 1.4, 1H), 7.97 (s, 1H, Ar), 8.17 (d, J = 8.2, 1H, Ar), 8.43 – 8.35 (m, 2H, Ar), 8.46 (d, J = 5.7, 1H, Ar), 9.14 (d, J = 1.8, 1H, Ar), 9.40 (s, 1H, Ar).

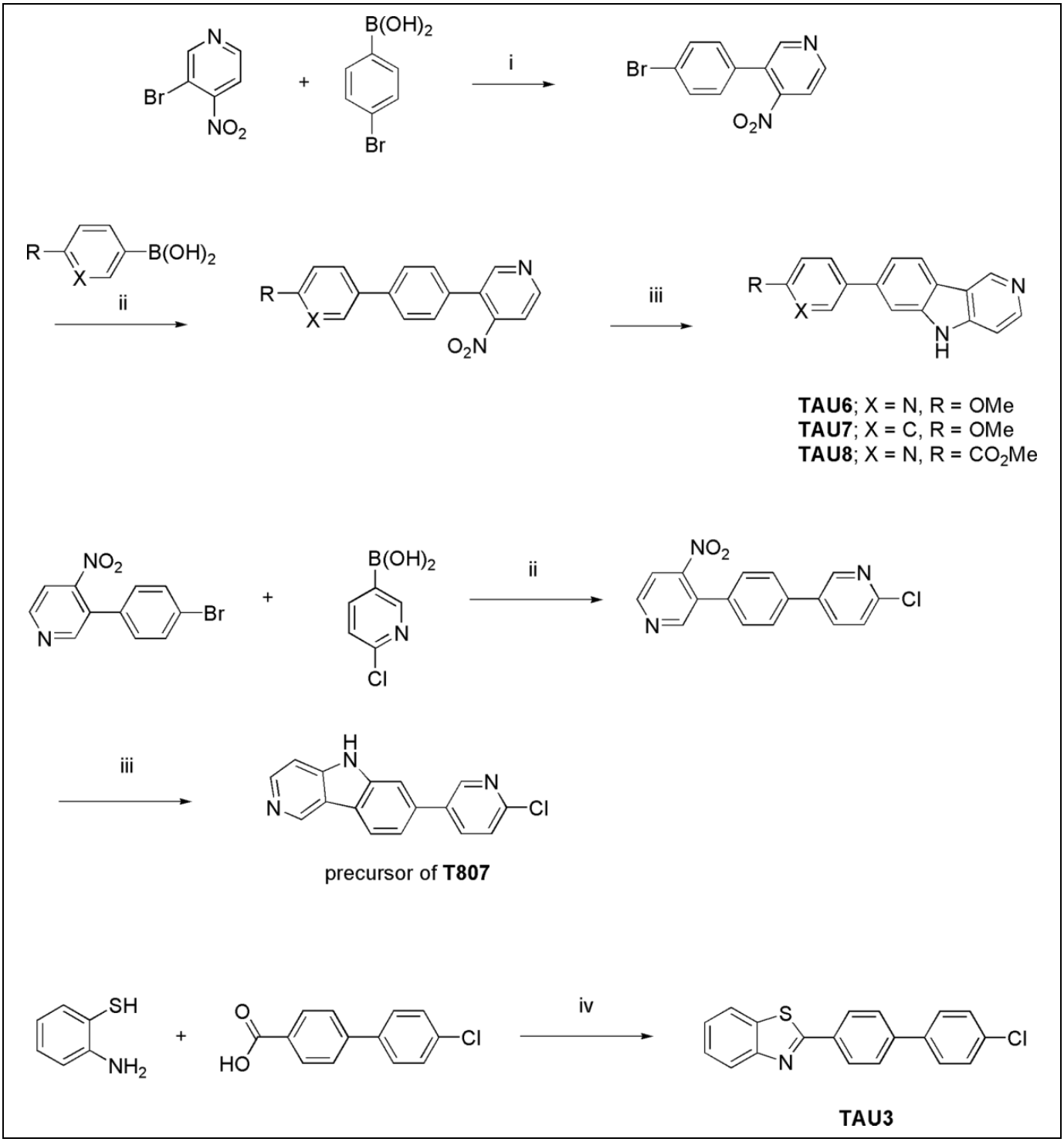

Figure 1. Synthesis of TAU3, TAU6-8, and the precursor of T807. i = $Pd(dppf)Cl_2/Na_2CO_3$, ACN, 80°C, 16 h, ii = $Pd(PPh_3)_4/K_2CO_3$, dioxane:water (1:1), 90°C, 16 h, iii = $P(OEt)_3$, 100°C, 3 h, iv = phosphorus pentoxide/methanesulfonic acid (PPMA), 100°C, 1 h.

N-Methyl-4-(quinolin-2-yl)benzenamine (BF-158). Compound was synthesized according to a described procedure.[26] LC-HRMS (ESI) calculated for $C_{16}H_{15}N_2$ $[MH]^+$ 234.1230, measured 235.1241; ^1H NMR (400 MHz, MeOD-*d4*) δ 2.86 (s, 3H, *N*-CH_3), 6.75 (d, $J = 8.3$, 2H, Ar), 7.50 (t, $J = 7.4$, 1H, Ar), 7.71 (t, $J = 7.4$, 1H), 7.81 to 8.08 (m, 5H, Ar), 8.27 (d, $J = 8.6$, 1H, Ar).

7-(6-chloropyridin-3-yl)-5H-pyrido[4,3-b]indole (precursor for T807).

Step 1: A mixture of 3-(4-bromophenyl)-4-nitro-pyridine[21] (0.70 g, 2.51 mmol), (4-chloro-3-pyridyl) boronic acid (0.592 g, 3.76 mmol), and potassium carbonate (0.693 g, 5.02 mmol) in 1,4-dioxane (14 mL) and water

(14 mL) was degassed under N_2 flow for 10 minutes. Then, tetrakis(triphenylphosphine)palladium^0 (0.145 g, 0.125 mmol) was added and the mixture was heated at 140°C for 10 minutes under microwave irradiation. The reaction mixture was diluted with dichloromethane and washed with water. The organic layer was separated, dried ($MgSO_4$), filtered, and the solvent was removed in vacuo. The residue was purified by flash chromatography (silicagel: ethyl acetate in heptane 0/100 to 40/60). The desired fractions were collected and the solvents removed in vacuo to give 2-chloro-5-[4-(4-nitro-3-pyridyl)phenyl]pyridine (0.34 g, 43% yield) as a pale yellow solid that was used as such for the next reaction step.

Step 2: A solution of 2-chloro-5-[4-(4-nitro-3-pyridyl)-phenyl]pyridine (0.30 g, 0.96 mmol) in triethyl phosphite (3 mL, 17.5 mmol) was heated at 100°C for 3 hours in a sealed tube. After this time, the mixture was cooled to 0°C and the precipitate filtered off and washed with cold diethyl ether. The solid was purified by flash chromatography (silicagel: MeOH/NH_3 in dichloromethane 0/100 to 04/96). The desired fractions were collected, the solvents were removed in vacuo, and the residue was triturated with diethyl ether to yield 7-(6-chloropyridin-3-yl)-5H-pyrido[4,3-b]indole (0.13 g, 48% yield) as a pale yellow solid (Figure 1). LC-HRMS (ESI) calculated for $C_{16}H_{10}ClN_3$ $[MH]^+$ 279.0563, measured 279.0567; ^{1}H NMR (400 MHz, DMSO-d6) δ 7.51 (dd, $J = 5.7$ and 0.9, 1H, Ar), 7.64 (dd, $J = 8.2$ and 1.7, 1H, Ar), 7.65 (d, $J = 8.4$, 1H, Ar), 7.88 (d, $J = 1.1$, 1H, Ar), 8.27 (d, $J = 8.2$ and 2.7, 1H, Ar), 8.36 (d, $J = 8.4$, 1H, Ar), 8.45 (d, $J = 5.5$, 1H, Ar), 8.85 (d, $J = 2.9$, 1H, Ar), 9.39 (s, 1H, Ar), 11.88 (s, 1H, NH).

Radiolabeling

2-[4-(2-[^{18}F]fluoroethyl)piperidin-1-yl]pyrimido[1,2-a]benzimidazole (AV-680, [^{18}F]T808), 7-[6-[^{18}F]fluoropyridin-3-yl]-5H-pyrido-[4,3-b]indole (AV-1451, [^{18}F]T807) and 2-[4-([^{11}C]methylamino)phenyl]benzothiazol-6-ol ([^{11}C]PiB). Fluorine-18 in the form of fluoride ([^{18}F]F^-) was produced by an ^{18}O(p,n)^{18}F nuclear reaction in a Cyclone 18/9 cyclotron (Ion Beam Applications, Louvain-la-Neuve, Belgium) by irradiation of 2 mL of 97% enriched ^{18}O-H_2O (Rotem HYOX18, Rotem Industries, Beer Sheva, Israel) using 18-MeV protons. After irradiation, [^{18}F]F^- was trapped on a SepPak Light Accell plus QMA anion exchange cartridge (CO_3^{2-} form, Waters, Milford, Massachusetts) and eluted with a mixture of Kryptofix 2.2.2 (K-222, 27.86 mg) and K_2CO_3 (2.46 mg) dissolved in CH_3CN/H_2O (0.75 mL; 95:5 v/v). After evaporation of the solvent with a stream of helium at 110°C, anhydrous CH_3CN (1 mL) was added, and [^{18}F]F^- was further dried under the same conditions. A solution of the precursor in DMSO (2 mg O-mesyl precursor in 0.6 mL for [^{18}F]T808 and 2 mg chloro precursor in 0.8 mL for [^{18}F]T807) was added to the dried [^{18}F]F^-–K_2CO_3–K-222 complex, and the mixture was heated at 90°C for 10 minutes (conventional heating) for [^{18}F]T808 and at 130°C and 50 W for 15 minutes (microwave cavity) for [^{18}F]T807. The crude radiolabeling mixture was diluted with 0.6 mL milliQ water (Millipore, Bedford, USA) and purified using reverse-phase HPLC (RP-HPLC) on an XBridge C_{18} column (5 µm, 4.6 × 150 mm; Waters) eluted with a mixture of 0.05 mol/L NaOAc pH 5.5 and EtOH (80:20 v/v for [^{18}F]T808 and 78:22 v/v for [^{18}F]T807) at a flow rate of 1 mL/min and with UV detection at 254 nm. [^{18}F]T808 and [^{18}F]T807 eluted at 21 and 16 minutes, respectively. [^{18}F]T807 was further purified on a SepPak Alumina N Plus Light cartridge (Waters). The purified radiotracer solution was diluted with saline to obtain an ethanol concentration <10%, suitable for intravenous injection. Quality control was performed using RP-HPLC on an XBridge column (C_{18}, 3.5 µm, 3.0 mm × 100 mm; Waters) eluted with a mixture of 0.05 mol/L NaOAc, pH 5.5, and CH_3CN (80:20 v/v for [^{18}F]T808 and 83:17 v/v for [^{18}F]T807) at a flow rate of 0.8 mL/min. UV detection was performed at 254 nm. [^{18}F]T808 and [^{18}F]T807 eluted at 8 and 7 minutes, respectively. [^{11}C]PiB was radiolabeled according to a published procedure.[27]

[^{3}H]-2-[4-(2-fluoroethyl)piperidin-1-yl]pyrimido[1,2-a]benzimidazole ([^{3}H]T808). 7-Bromo-2-[4-(2-fluoroethyl)piperidin-1-yl]pyrimido[1,2-a]benzimidazole (1.00 mg, 2.65 µmol) was dissolved with *N,N*-Diisopropylethylamine DIPEA (2 µL, 11.47 µmol) in methanol MeOH (0.25 mL, 6.18 mmol). Palladium (1.00 mg, 0.94 µmol) was added, and the mixture was degassed thoroughly three times and placed under tritium atmosphere and allowed to reach room temperature while stirring for 30 minutes. Next, the tritium gas was diverted to a waste trap, and volatiles were lyophilized to a waste vial. The reaction product was quenched three times with 150 µL MeOH to remove labile tritium atoms, and the solvent was lyophilized to a waste vial. Then, the reaction product was filtered over an acrodisc (Pall 1-mm syringe filter) and dissolved in 10 mL EtOH. Ten µL of the final product was diluted in 10 mL MeOH of which 10 µL was counted in 3 mL liquid scintillation counter LSC (253.4 MBq/mL). The crude mixture was purified using RP-HPLC.

[^{3}H]-N-[4-[2(E)-[6-[2-[2-(2-fluoroethoxy)ethoxy]ethoxy]pyridin-3-yl]vinyl]pheny]-N-methylamine (AV-45, [^{3}H]florbetapir). N-[4-[2(E)-[6-[2-[2-(2-fluoroethoxy)ethoxy]ethoxy]pyridin-3-yl]vinyl]pheny]-N-methylamine (0.42 mg, 1.17 µmol) was dissolved in dichloromethane DCM with [(cod)Ir(Py)(PCy3)]PF6 (0.78 mg, 0.97 µmol). The mixture was thoroughly degassed in liquid N_2 and placed under 150 mbar tritium for 1 hour at room temperature, reaching 838 mbar. The diluted gas was trapped on the waste bed, and the solvent waste was lyophilized to the waste vial and rinsed via lyophilization three times with MeOH. Afterward, the residue was dissolved in 10 mL EtOH. Ten µL of the latter solution was diluted in 10 mL MeOH, of

which 10 μL was counted in 3 mL LSC (534.6 MBq/mL). The crude mixture was purified using RP-HPLC.

Biodistribution Studies

Biodistribution of [^{18}F]T808 and [^{18}F]T807 was studied in healthy male Naval Medical Research Institute (NMRI) mice (body weight: 30-40 g) at 2, 10, 30, and 60 minutes postinjection (PI; $n = 4$/time point). Mice were anesthetized (2.5% isoflurane in O_2 at 1 L/min flow rate) and injected with about 0.9 MBq of the tracer via a tail vein and killed by decapitation at above-specified time points. Blood and major organs were collected in tared tubes and weighed. Radioactivity in blood, organs, and other body parts was counted using an automated γ-counter. For the calculation of total radioactivity in blood, bone, and muscle, masses were assumed to be, respectively, 7%, 12%, and 40% of the total body mass.

Radiometabolites

Plasma radiometabolites. The NMRI mice were anesthetized with isoflurane (2.5% in O_2 at 1 L/min flow rate) and injected with [^{18}F]T808 or [^{18}F]T807 (~3.7 MBq) via a lateral tail vein. They were killed by decapitation at 2, 10, 30, or 60 minutes PI ($n = 3$/time point). Blood was collected in EDTA-containing tubes (4 mL tubes; BD vacutainer, BD, Franklin Lakes, New Jersey) and stored on ice. Blood was subsequently centrifuged at 2330 $\times g$ for 10 minutes to separate the plasma. Plasma (0.5 mL) was isolated and spiked with 10 μg of authentic T808 or T807 and analyzed by HPLC (Chromolith C_{18}, 3.0 × 100 mm; Merck, Darmstadt, Germany) and eluted with gradient mixtures of 0.05 mol/L NaOAc pH 5.5 (A) and CH_3CN (B; 0-4 minutes: isocratic 0% B, 0.5 mL/min; 4-14 minutes: linear gradient 0% B to 90% B, 1 mL/min; 14-17 minutes: isocratic 90% B, 1 mL/min). After passing through a UV detector at 254 nm coupled in series with a 3-in NaI(Tl) scintillation detector and connected to a single-channel analyzer, the HPLC eluate was collected as 1 mL fractions (model 2110 fraction collector; Biorad, Hercules, California). The radioactivity of fractions was counted in an automated γ-counter.

Perfused brain radiometabolites. For each time point, three NMRI mice were injected with [^{18}F]T808 or [^{18}F]T807 (~7.4 MBq). At 10 or 60 minutes PI, the mice were killed by an overdose of pentobarbital (Nembutal; CEVA Santé Animale, Brussels, Belgium; 150 mg/kg intraperitoneally) and perfused with saline via the left ventricle. Brain was isolated and homogenized in CH_3CN (2 mL). After centrifugation at 3000 rpm (1310× g) for 5 minutes, the supernatant (~1 mL) was collected, diluted with H_2O (1 mL), and filtered through a 0.22-μm filter (Millipore, Bedford, Massachusetts). About 0.5 mL of the filtrate was further diluted with an equal volume of H_2O and spiked with 20 μg authentic T808 or T807 before being analyzed on an analytical XBridge column (C_{18}, 3.5 μm, 3.0 × 100 mm; Waters) and eluted with a mixture of 0.05 mol/L NaOAc pH 5.5 and CH_3CN (80:20 v/v for [^{18}F]T808 and 85:15 v/v for [^{18}F]T807) at a flow rate of 0.8 mL/min. Ultraviolet detection was done at 254 nm. The HPLC eluate was collected as 1 mL fractions, and their radioactivity was counted in an automated γ-counter.

Immunohistochemistry

Human brain slices. Frozen sections were stained using Dako automated stainer (DakoCytomation, Glostrup, Denmark), using antisera generated against Aβ (M0872—clone 6F/3D; DakoCytomation, Glostrup, Denmark; 1:100 dilution) and Tau (T6402; Sigma Aldrich, St Lous, Missouri; 1:250 dilution), according to the manufacturer's protocol.

Mouse brain slices. Transgenic mice expressing mutant human P301L tau were killed by decapitation, brains were removed from the skull, snap frozen in 2-methylbutane (−30°C), and stored at −20°C until 20-μm thick sections were sliced for immunohistochemistry. Sections were dried, fixed in formalin, and incubated with hydrogen peroxide (Vector labs, Burlingame, California; S2023) for 5 minutes and blocking reagent during 1 hour (mouse-on-mouse [MOM] kit; Vector labs; BMK-2202). Anti-AT8 antibody (in-house, 0.2 μg/mL in MOM diluent) was applied to the sections overnight. Next day, the slices were incubated with horseradish peroxidase-conjugated antimouse secondary antibody (Envision; DAKO, Glostrup, Denmark; K4000), followed by chromogenic diamino benzene labeling (DAKO, K3468). After counterstaining with hematoxylin, sections were dehydrated and mounted with organic mounting medium (Vectamount, Vector labs; H-5000).

In Vitro Autoradiography Binding Inhibition Studies

Air-dried, frozen, 10-μm thick slices of the visual cortex of an patient with AD (68-year old female with Braak stage V-VI) were incubated for 60 minutes with [^{18}F]T808 or [^{18}F]T807 (0.74 MBq/500 μL per section) and subsequently washed with mixtures of phosphate-buffered saline (PBS) and ethanol as described elsewhere.[11] In the case of [^{11}C]PiB, slices were incubated with 0.37 MBq/500 μL per section for 10 minutes. To assess specificity of binding, slices were incubated with tracer in the presence of 1 μmol/L of authentic T808, T807, astemizole, lansoprazole, THK-5105, BF-158, BF-170, TAU1-8, or PiB. After drying, the slices were exposed to a phosphor storage screen (super-resolution screen; Perkin Elmer, Waltham, Massachusetts). Screens were read in a Cyclone Plus system (Perkin Elmer) and analyzed using Optiquant software (Perkin Elmer). Results are expressed as digital light units per square mm (DLU/mm^2). Adjacent AD slices were immunostained with anti-tau (T6402) and anti-Aβ antibodies (6F/3D), as described earlier, to correlate with [^{18}F]T808, [^{18}F]T807, or [^{11}C]PiB binding. Slices of the P301L-transgenic mice and their wild-type controls were analyzed in similar manner using

[^{18}F]T808 (0.74 MBq/500 μL per section) and 1 μmol/L of cold T808.

PHF Tau and Amyloid Plaques Isolation From Human AD Brain

Enriched paired helical filaments PHF tau fractions were prepared according to a slightly modified version of the protocol described by Greenberg and Davies[28] using human AD brain tissue (occipital cortex with high tau fibril load). Briefly, frozen human AD brain samples ($\sim$10 g) were homogenized with 10 volumes of cold homogenization buffer (10 mmol/L Tris, 800 mmol/L NaCl, 1 mmol/L ethylene glycol tetraacetic acid EGTA, 10% sucrose, pH 7.4) containing PhosSTOP phosphatase and cOmplete EDTA-free protease inhibitor (Roche, Vilvoorde, Belgium) on ice. After centrifugation at 27.000 $\times$ *g* for 20 minutes at 4°C, the supernatant was recovered and 1% (w/v) N-lauroylsarcosine and 1% (v/v) 2-mercaptoethanol were added. The N-lauroylsarcosine/2-mercaptoethanol supernatant was incubated for 2 hours at 37°C while shaking on an orbital shaker. Subsequently, ultracentrifugation at 108.000 $\times$ *g* for 1.5 hours at room temperature enriched PHF tau in the pellet. Supernatant was removed, and the pellet was carefully rinsed twice with a small volume of Tris-buffered saline (TBS; 50 mmol/L Tris, 150 mmol/L NaCl, pH 7.4). Finally, the PHF tau pellet was recovered in TBS and resuspended to ensure sample homogeneity. Small aliquots were stored at −80°C.

Frozen human AD brain samples (10 g—occipital cortex with high amyloid plaques load) were homogenized with a 7-fold volume of cold homogenization buffer (250 mmol/L sucrose, 20 mmol/L Tris base, 1 mmol/L EDTA, 1 mmol/L EGTA, and PhosSTOP phosphatase and cOmplete EDTA-free protease inhibitor) on ice. After centrifugation at 27.000 $\times$ *g* for 20 minutes at 4°C, cell debris was removed. Supernatant containing amyloid plaques was aliquoted and stored at −80°C.

In Vitro Competitive Radioligand Binding Assays

The competitive radioligand binding assays measure the binding of a radiolabeled reference ligand in the presence of a dose–response concentration range of test compounds T807, T808, lansoprazole, astemizole, PiB, THK5105, TAU1, and TAU4-8 (TAU2-3 were not evaluated due to solubility problems).

Briefly, PHF tau preparations were diluted to 100 μg protein/mL in PBS buffer with 5% ethanol. In a 96-well format, ^{3}H-T808 (specific activity 1 GBq/μmol) was added at a final concentration of 10 nmol/L to increasing amounts of test compound in the presence of 20 μg protein of PHF tau preparation. Nonspecific binding was defined as the number of counts remaining in the presence of 50 μmol/L thioflavin T (common beta sheet binder). After 2 hours incubation at room temperature, the unbound ligand was removed by filtration of the binding mixtures over GF/B glass filters using a Filtermate 96 harvester instrument (Perkin Elmer, Zaventem, Belgium). The filters were washed three times with PBS buffer containing 20% ethanol. After overnight drying of the filter plate, Microscint O liquid (Perkin Elmer) was added, and the amount of radiolabeled ligand bound to the fibrils was measured by liquid scintillation counting in a Topcount instrument (Packard Instrument, Meriden, Connecticut).

Values for half-maximal inhibitory concentration (IC_{50}) were determined from displacement curves of at least two independent experiments using GraphPad Prism software (GraphPad Software, San Diego, California).

To determine compound binding to the amyloid plaques, a similar assay was put in place but with some minor modifications. Briefly, amyloid preparations were diluted to 150 μg protein/mL in 50 mmol/L Tris with 0.1% bovine serum albumin (BSA) and 5% ethanol. ^{3}H-AV-45 (florbetapir—specific activity 2 GBq/μmol) was added at a final concentration of 10 nmol/L to increasing amounts of test compound in the presence of 30 μg protein of amyloid plaques preparation. Nonspecific binding was determined in the presence of 500 μmol/L thioflavin T. After 150 minutes incubation at room temperature, the binding mixtures were filtered over GF/B glass filters. The filters were washed three times with PBS buffer containing 20% ethanol. Subsequent steps were identical to those described for the PHF tau preps.

Results

Radiolabeling

[^{18}F]T808 and [^{18}F]T807 were synthesized by a nucleophilic substitution reaction on their corresponding mesyl and chloro precursor with [^{18}F]fluoride in DMSO (Figures 2 and 3). Heating of the precursor solution in the presence of K-222/K_2CO_3 afforded [^{18}F]T808 and [^{18}F]T807 with an average, decay-corrected, radiochemical yield of 21% and 6%, respectively (relative to radioactivity of [^{18}F]F^- in the preparative chromatogram, $n = 7$). Purification of the crude radiolabeling reaction mixture was done on an isocratic RP-HPLC system using a mixture of acetate buffer and ethanol as mobile phase. Radiochemical purity was examined using HPLC on an analytical C_{18} column and was more than 99%. Both tracers were obtained within a total synthesis time of 60 minutes and were collected with an average specific radioactivity of 119 GBq/μmol at the end of synthesis (EOS, $n = 7$) for [^{18}F]T808 and 50 GBq/μmol at EOS ($n = 7$) for [^{18}F]T807. [^{11}C]PiB had a mean specific activity of 85 GBq/μmol at EOS and a radiochemical purity of $\geq$99% ($n = 2$).

Biodistribution in Normal Mice

Table 1 shows the percentage of injected dose per gram (%ID/g) of [^{18}F]T808 and [^{18}F]T807 in different organs at 2, 10, 30, and 60 minutes PI. Clearance from blood, defined as the 2 minutes to 60 minutes activity ratio, was slower for [^{18}F]T807 (2.5) than for [^{18}F]T808 (2.7). Both tracers were mainly cleared via the hepatobiliary system into the intestines

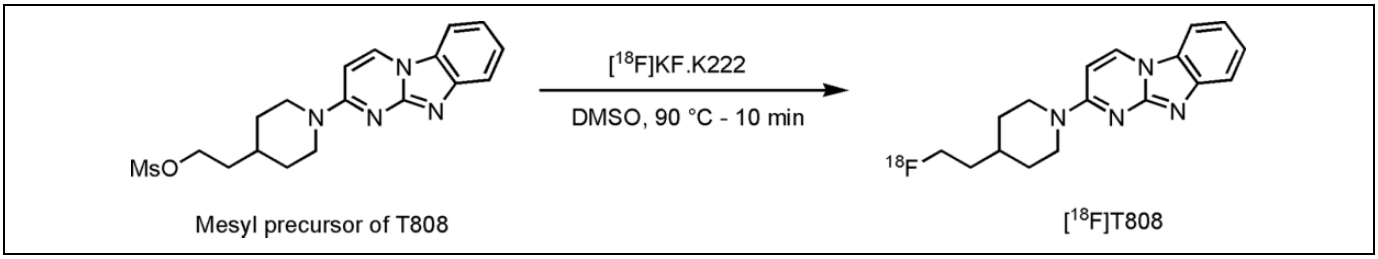

Figure 2. Radiolabeling of T808.

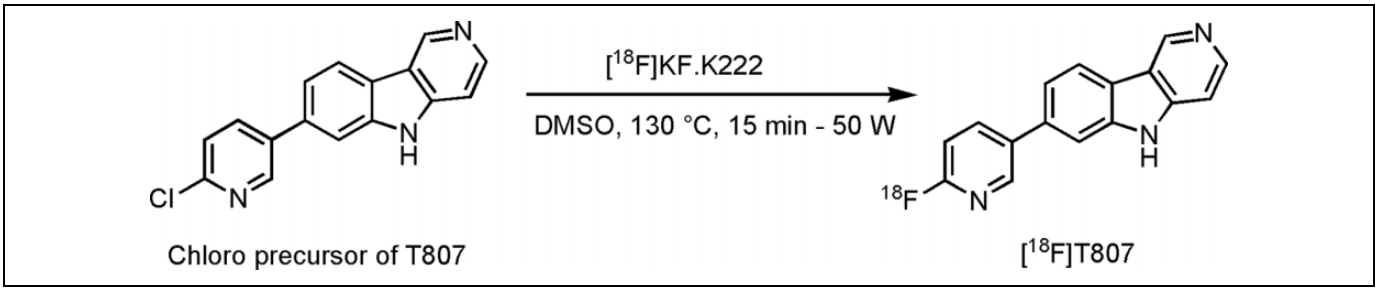

Figure 3. Radiolabeling of T807.

Table 1. Biodistribution of [^{18}F]T808 and [^{18}F]T807 in Normal Mice at 2, 10, 30, and 60 Minutes PI.

	%ID/g[a]							
	[^{18}F]T808				[^{18}F]T807			
Body part	2 min	10 min	30 min	60 min	2 min	10 min	30 min	60 min
Blood	1.8 ± 0.1	2.0 ± 0.2	1.5 ± 0.1	0.7 ± 0.1	1.5 ± 0.2	0.7 ± 0.0	0.7 ± 0.1	0.6 ± 0.1
Bone	2.6 ± 0.6	4.2 ± 0.6	10.2 ± 2.8	9.2 ± 6.1	0.1 ± 0.1	1.4 ± 0.2	0.0 ± 0.0	0.1 ± 0.0
Brain	4.9 ± 0.5	0.9 ± 0.3	0.4 ± 0.0	0.3 ± 0.0	7.5 ± 1.1	2.6 ± 0.5	0.8 ± 0.4	0.4 ± 0.2
Cerebellum	5.2 ± 0.5	1.0 ± 0.6	0.6 ± 0.1	0.5 ± 0.2	8.5 ± 1.4	2.4 ± 0.5	0.8 ± 0.4	0.4 ± 0.2
Cerebrum	4.9 ± 0.5	1.0 ± 0.1	0.4 ± 0.0	0.2 ± 0.0	7.2 ± 1.0	2.6 ± 0.5	0.8 ± 0.4	0.4 ± 0.2
Heart	3.2 ± 0.4	2.3 ± 0.3	1.7 ± 0.0	0.8 ± 0.1	6.8 ± 0.9	2.1 ± 0.3	1.3 ± 0.3	1.0 ± 0.1
Kidneys	26.3 ± 1.7	12.7 ± 1.7	9.2 ± 2.3	3.6 ± 1.7	35.9 ± 6.2	25.6 ± 3.0	15.8 ± 5.0	13.0 ± 2.6
Liver	11.8 ± 2.4	15.1 ± 1.6	8.3 ± 1.2	4.2 ± 0.7	12.6 ± 2.4	14.6 ± 1.0	20.7 ± 1.8	18.1 ± 2.2
Lungs	4.8 ± 0.6	3.0 ± 0.3	1.8 ± 0.2	0.9 ± 0.2	25.1 ± 11.9	4.2 ± 1.8	3.9 ± 1.2	2.1 ± 0.7
Muscle	1.5 ± 0.5	1.0 ± 0.2	0.8 ± 0.1	3.5 ± 5.5	3.0 ± 1.8	1.4 ± 0.3	0.6 ± 0.1	0.5 ± 0.1
Pancreas	7.3 ± 2.4	4.0 ± 2.0	2.2 ± 0.5	1.2 ± 0.3	4.1 ± 2.2	4.7 ± 0.7	2.1 ± 0.8	1.5 ± 0.6
Spleen	16.6 ± 6.7	4.9 ± 0.6	2.4 ± 0.4	1.3 ± 0.3	15.7 ± 5.1	13.8 ± 12.5	3.8 ± 1.3	3.1 ± 1.7
	2/60 min				2/60 min			
Brain	18.2				18.3			
Blood	2.7				2.5			

Abbreviations: PI, postinjection; SD, standard deviation.
[a] Percentage of injected dose/gram, calculated as: (counts per minute in body part/sum of counts per minute in all body parts)/(weight of the individual organ). Data are expressed as mean ± SD; $n = 4$ per time point.

and to a lesser extent via the renal pathway. High initial brain uptake was observed (4.9%ID/g at 2 minutes PI for [^{18}F]T808 and 7.5%ID/g at 2 minutes PI for [^{18}F]T807) with fast washout (0.9%ID/g at 10 minutes PI for [^{18}F]T808 and 2.6%ID/g at 10 minutes PI for [^{18}F]T807). High 2 to 60 minutes activity ratios for the brain were therefore also found (18.2 for [^{18}F]T808 and 18.3 for [^{18}F]T807). In contrast to [^{18}F]T807, [^{18}F]T808 showed high bone uptake (up to 10%ID/g at 30 minutes PI) suggesting loss of fluorine 18 from the radioligand *in vivo*.

Radiometabolites

The plasma radiometabolite analysis of [^{18}F]T808 and [^{18}F]T807 in NMRI mice revealed rapid metabolism *in vivo*

Table 2. Relative Percentages of Intact Tracer at 2, 10, 30, and 60 Minutes After Injection of [^{18}F]T808 and [^{18}F]T807 in Plasma and Perfused Brain of Normal Mice.

Plasma	Mean % ± SD ($n = 3$) of intact tracer			
	2 min	10 min	30 min	60 min
T808	65 ± 8	34 ± 3	29 ± 3	26 ± 12
T807	99 ± 1	84 ± 5	60 ± 14	45 ± 4
Perfused brain	**Mean % ± SD (n = 3) of intact tracer**			
		10 min		60 min
T808		88 ± 2		34 ± 10
T807		100 ± 0		99 ± 1

Abbreviation: SD, standard deviation.

for [^{18}F]T808 and a relatively slow metabolism for [^{18}F]T807 (Table 2). At 2 minutes PI, only 65% of the recovered radioactivity of [^{18}F]T808 was still in the form of intact tracer, whereas [^{18}F]T807 remained intact (99%). At 30 minutes PI, the fraction of intact [^{18}F]T808 and [^{18}F]T807 decreased, respectively, to 29% and 60%. All detected radiometabolites were more polar than the intact tracers. The recovery of radioactivity for [^{18}F]T808 and [^{18}F]T807 was high, (respectively, 89% and 85% [$n = 12$]).

In brain, the percentage of intact [^{18}F]T808 decreased from 88% at 10 minutes PI to 34% at 60 minutes PI, while the fraction of parent [^{18}F]T807 in brain remained close to 100% at both 10 and 60 minutes PI (Table 2). The detected radiometabolites were more polar than the intact tracers, and no radiometabolites more lipophilic than the intact tracer were detected 60 minutes PI. The recovery of the HPLC column-injected radioactivity for [^{18}F]T808 and [^{18}F]T807 was 85% and 70%, respectively ($n = 6$).

In vitro Autoradiography Binding Studies

Digital autoradiography with [^{18}F]T808 and [^{18}F]T807 on human AD slices showed binding to tau-rich regions in the 1 to 3 cortical layers and 5 to 6 cortical layers of the visual cortex (Figure 4). Immunohistochemistry with tau and Aβ antibodies, performed on adjacent slices, identified numerous NFTs and neuritic plaque deposits, confirming colocalization of tracer binding with NFTs (Figure 5). To assess the specificity of the tracer binding to these NFTs, blocking studies with several tau-specific ligands and Aβ-specific ligands were performed. An overview of the different compounds used to block (at 1 μmol/L concentration) the binding of [^{18}F]T808, [^{18}F]T807, and [^{11}C]PiB is given in Table 3. These ligands are divided into 3 groups: reported ligands (group 1), newly developed ligands (group 2), and studies with [^{11}C]PiB (group 3). Binding of [^{18}F]T808 and [^{18}F]T807 to NFT-rich regions was reduced with 94% and 90% in the presence of 1 μmol/L T807 and T808, respectively. Self-blocking with 1 μmol/L of the cold ligand, on the other hand, resulted in 88% inhibition for T807 and 89% for T808. Self-blocking of [^{11}C]PiB[10] resulted in 57% blocking. More than 70% reduction in binding of [^{18}F]T808 or [^{18}F]T807 was observed with BF-158, BF-170, THK5105, TAU1, and TAU5-8 at a concentration of 1 μmol/L. With lansoprazole, astemizole, PiB, and TAU2-4 on the other hand, blocking was less pronounced (range 0%-59%). No significant inhibition (< 17%) of [^{11}C]PiB binding was observed with 1 μmol/L T808, T807, and TAU6-8. Finally, [^{18}F]T808 did not show any specific binding to murine tau in the P301L transgenic mouse model (Figure 6).

In vitro Competitive Radioligand Binding Assays

Table 4 shows the binding assays of [^{3}H]T808 with cold test compounds showing high affinity of reference compounds T807, T808, PiB, and THK-5105 for purified tau but low affinity of lansoprazole and astemizole (pIC_{50} equal to or higher than 6.49). Of the newly synthesized compounds, only TAU7 showed high affinity (pIC_{50} of 7.46), whereas TAU1, TAU4-6, and TAU8 showed low affinity ($pIC_{50} < 5$). In the competition assays with [^{3}H]AV-45, low affinity was recorded for T808, lansoprazole, and astemizole ($pIC_{50} < 5$). T807 and THK5105 showed specific binding with pIC_{50} values of 6.25 and 7.25, respectively. PiB had a pIC_{50} of 8.10. In the group of newly synthesized ligands, only TAU7 showed affinity with a pIC_{50} of 7.95, while the other TAU compounds had pIC_{50} values lower than <5.

Discussion

One of the aims of this study was to determine some important preclinical properties of [^{18}F]T808 and [^{18}F]T807, such as brain uptake, washout from brain, and formation of radiometabolites, since these ligands are among the most selective tau tracers with high affinity for NFTs reported in literature to date.[15] In addition, with a $clogD_{7.4}$ between 2.0 and 3.5, a polar surface area <80 Å^2, and a low molecular mass (<500 Da), both compounds show optimal molecular features for a passive transfer across the blood–brain barrier (BBB).[29] Although these tracers have already been evaluated in clinical trials,[18,19] preclinical data remain essential in the search for new and better ^{18}F- and ^{11}C-labeled imaging agents for tauopathies other than AD. Once we characterized [^{18}F]T808 and [^{18}F]T807 as benchmark compounds, both compounds were used in semiquantitative autoradiography experiments to evaluate and compare binding characteristics of recently reported tau tracers and newly synthesized radioligands.

Although the radiosynthesis of both [^{18}F]T808 and [^{18}F]T807 has been described with relative high specific activities and radiochemical yields,[8,11] we have put low effort in optimization of their labeling process, as this was not required for the type of experiments we performed.

The biodistribution of [^{18}F]T808 and [^{18}F]T807 in normal mice revealed high initial brain uptake with rapid washout after 10 minutes. In contrast to [^{18}F]T807, pronounced accumulation of radioactivity in bone was observed for [^{18}F]T808, likely due to defluorination *in vivo*.[19] These results were expected based

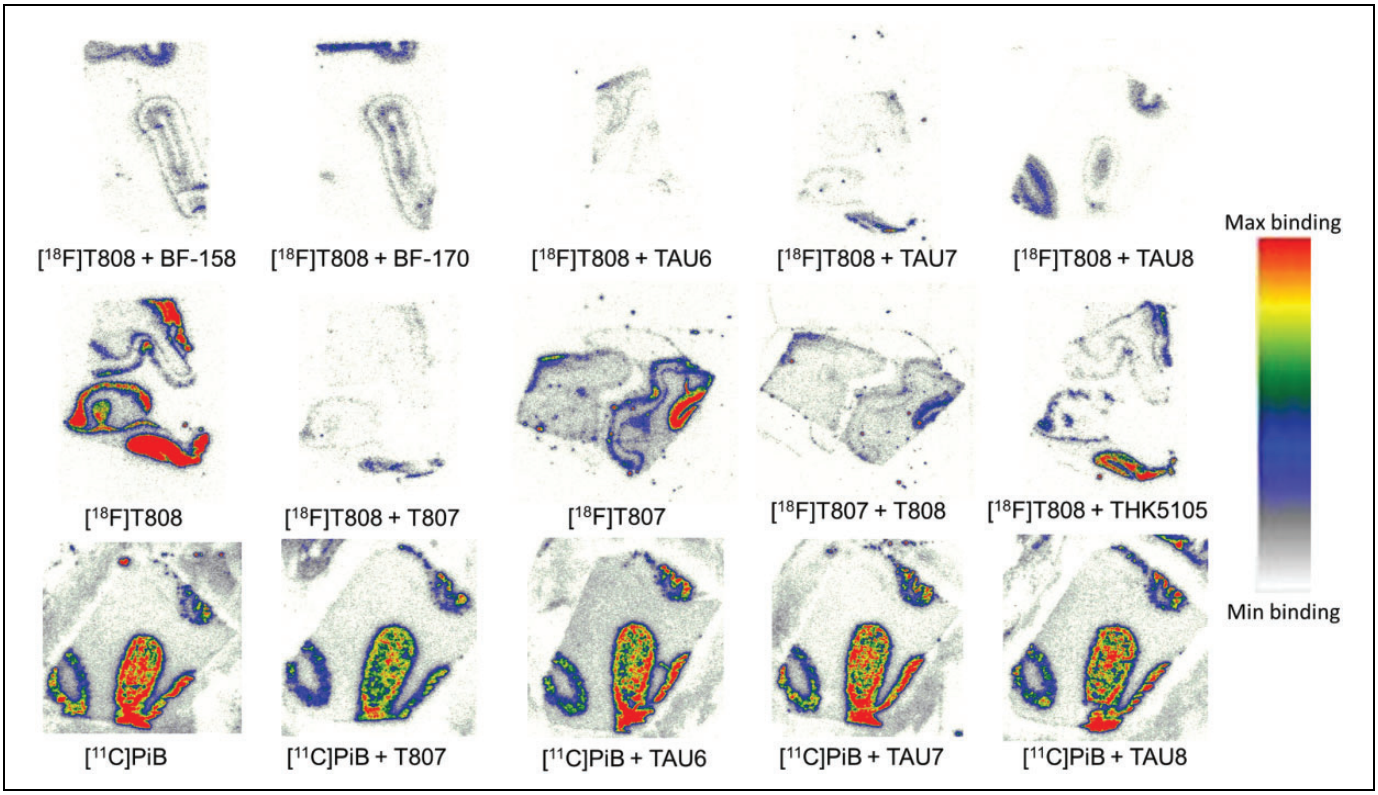

Figure 4. Human Alzheimer disease (AD) brain slices incubated with [^{18}F]T808, [^{18}F]T807, and [^{11}C]PiB in the presence of authentic reference ligands and newly developed compounds at 1 mmol/L. Slices with [^{18}F]T808 and [^{18}F]T807 are from different experiments.

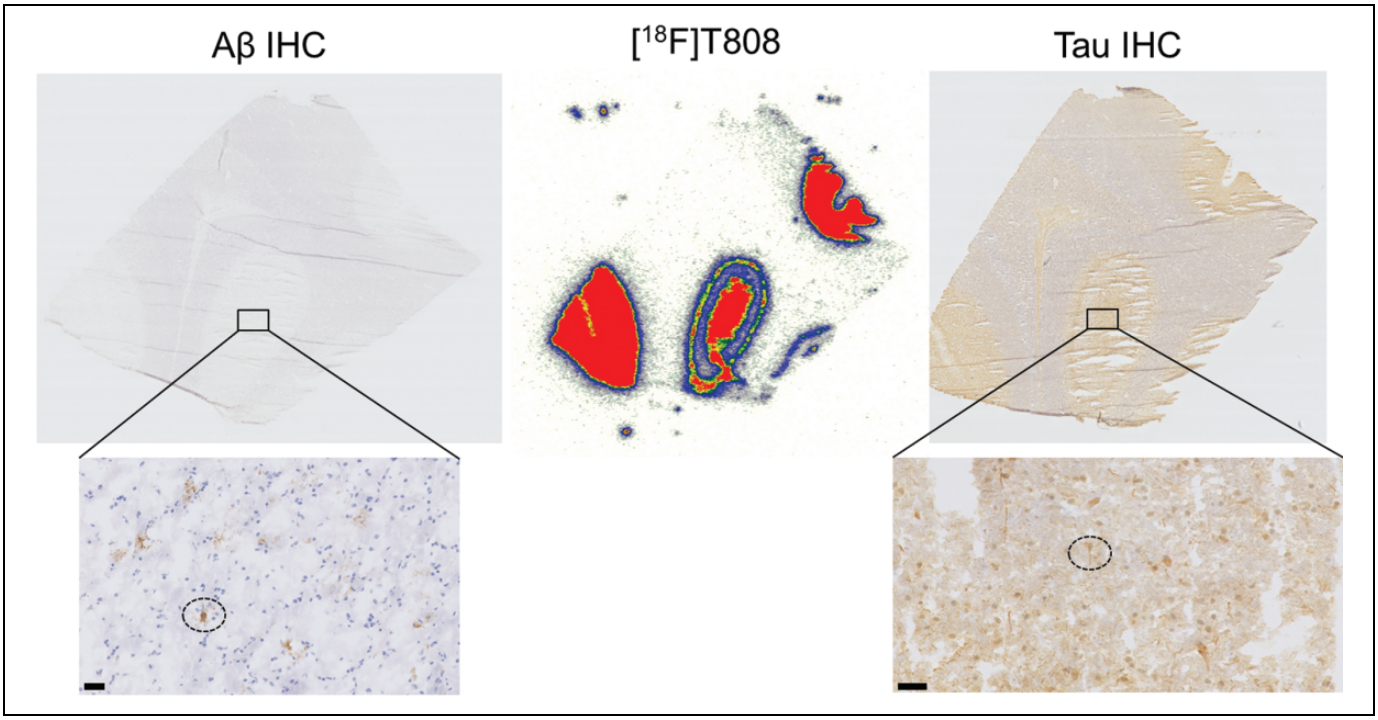

Figure 5. Autoradiography analysis on 10-mm thick slices of the visual cortex of an patient with Alzheimer disease (AD; 68-year-old female with Braak stage V-VI) with [^{18}F]T808 (autoradiogram in the middle). Adjacent slices were immunostained with tau (T6402) on the right and amyloidbeta (Ab; M0872) on the left. Higher magnification on the bottom identifies tau tangles and amyloid plaques (dotted circles). Scale bar: 50 mm.

Table 3. Percentage Blocking of Tracer Binding for [^{18}F]T808, [^{18}F]T807, and [^{11}C]PiB in the Presence of Several Compounds With Affinity for tau or Aβ.

Group	Compound (1 μmol/L)	nmol/L Tracer (^{18}F + ^{19}F / ^{11}C + ^{12}C)	% Block ± SD ($n = 3$)[a]
1	T807	28 [^{18}F]T807	88 ± 0.0
	T808	7 [^{18}F]T808	89 ± 0.0
	T807	7 [^{18}F]T808	94 ± 0.0
	T808	28 [^{18}F]T807	90 ± 10[b]
	BF-158	40 [^{18}F]T808	93 ± 0.0
	BF-170	40 [^{18}F]T808	84 ± 0.1
	Lansoprazole	40 [^{18}F]T808	4 ± 0.5
	Astemizole	40 [^{18}F]T808	22 ± 0.4
	PiB	7 [^{18}F]T808	19 ± 0.1
	THK5105	7 [^{18}F]T808	78 ± 0.0
2	TAU1	7 [^{18}F]T808	75 ± 0.1
	TAU2	10 [^{18}F]T808	48 ± 0.0
	TAU3	10 [^{18}F]T808	29 ± 0.1
	TAU4	10 [^{18}F]T808	47 ± 0.0
	TAU5	10 [^{18}F]T808	73 ± 0.0
	TAU6	10 [^{18}F]T808	94 ± 0.0
	TAU7	7 [^{18}F]T808	91 ± 0.0
	TAU8	43 [^{18}F]T808	90 ± 0.0
3	PiB	13 [^{11}C]PiB	57 ± 0.0
	T807	13 [^{11}C]PiB	11 ± 0.1
	T808	66 [^{11}C]PiB	17 ± 0.0
	TAU6	13 [^{11}C]PiB	0 ± 0.1
	TAU7	13 [^{11}C]PiB	0 ± 0.0
	TAU8	13 [^{11}C]PiB	0 ± 0.1

Abbreviations: Aβ, amyloid β; DLU/mm^2, digital light units per square mm; SD, standard deviation.

[a] Calculated as (DLU/mm^2 in the presence of 1 μmol/L blocker) / (DLU/mm^2 tracer only).

[b] SD values of three different experiments. Other SD values are on three different slices in one and the same experiment.

on the μ-PET biodistribution data from the original report on [^{18}F]T808.[8] The μPET data suffer however from limited resolution when compared to an *in vivo* biodistribution study in which the radioactivity of individual organs is counted after dissection, and thus results of the two approaches are only partly comparable. *Ex vivo* biodistribution data of [^{18}F]T808 and [^{18}F]T807 are therefore important as benchmark data in order to compare performance of new potential tau tracers.

We quantified the fraction of radiometabolites of [^{18}F]T808 and [^{18}F]T807 in plasma and perfused brain of normal mice. In plasma, metabolism was relatively fast for [^{18}F]T808, compared to [^{18}F]T807. One major polar radiometabolite was detected for each tracer. In view of the observed bone uptake in the biodistribution study, [^{18}F]T808's main radiometabolite is therefore probably [^{18}F]fluoride. This might lead to inaccurate quantification of tracer binding in brain, in view of partial volume effects. Early clinical PET imaging results with [^{18}F]T808 showed however no interference with image interpretation at early time points.[19] In brain, ideally no radiometabolites should be present, since they may have different brain kinetics and brain distribution than the parent compound and thus complicate tracer modeling and PET quantification. In their original article on preclinical properties of [^{18}F]T808, Zhang et al mention the absence of radiometabolites in mouse brain.[8] Metabolic stability was however conducted in liver microsomal assays of mice and humans, where rapid metabolism was shown (in the presence of cofactor NADPH) 60 minutes after incubation. Furthermore, while polar metabolites might not always cross the BBB, *ex vivo* brain metabolite studies should confirm this. We therefore performed *ex vivo* brain metabolite studies in mice, which showed the presence of two unidentified polar radiometabolites the fraction of which is 66% at 60 minutes PI (see Table 2). Further, *in vitro* brain radiometabolite analysis is required to determine whether metabolism is peripheral with subsequent passage of the radiometabolite through the BBB and/or whether it occurs within the brain.

In the second part of this study, we performed a semiquantitative autoradiography screening with [^{18}F]T808 and [^{18}F]T807 as reference tracers, in combination with several tau-specific ligands reported in the literature (group 1 in Table 3) and with newly synthesized ligands containing structural moieties with known affinity for tau, such as benzothiazoles, carbazoles, and phenylthiazolylhydrazide compounds (group 2 in Table 3). Similar autoradiography studies were also performed with [^{11}C]PiB to examine the selectivity of several compounds for Aβ (group 3 in Table 3). Furthermore, we examined pIC_{50} values of several compounds in competition binding assays with [^{3}H]T808 and [^{3}H]AV-45 on purified tau and Aβ from patients with AD (Table 4). These binding studies provide additional, quantitative information on the affinity of several cold compounds for purified human tau and Aβ, but the absence of off-target binding should also be taken into account when comparing the results of autoradiography blocking studies on AD slices. Overall, the screening assays provide valuable information on the nature of structural moieties necessary for binding to tau fibrils and thus can be very helpful in the development of new specific high-affinity ligands for tau.[8,11] The disadvantage of using a particular radioligand in the autoradiography studies, [^{18}F]T808 in our case, to screen for new compounds with high affinity for tau is that allosteric binding is overlooked, and only compounds that bind to identical regions of tau are detected. An alternative approach to screen for new tau selective compounds could be the use of fluorescent dyes such as thioflavin or congo red derivatives. Such compounds emit a stronger fluorescent signal when interacting with beta-sheet aggregates, making quantification challenging. Furthermore, these derivatives show affinity for many different misfolded proteins with beta-sheet structures and are therefore less specific to screen for tau ligands. Thus, using the highly selective and specific tau tracer [^{18}F]T808, we specifically screened for compounds with affinity for aggregated tau beta sheets. The *in vitro* autoradiography and immunohistochemistry studies with human AD brain sections showed preferential binding of [^{18}F]T808 and [^{18}F]T807 to tau fibrils in the cortical layers of the visual cortex, where large amounts of NFTs and neuropil thread deposits are to be expected, based on the literature.[30,31] Displacement of [^{18}F]T808 by T807 was more pronounced

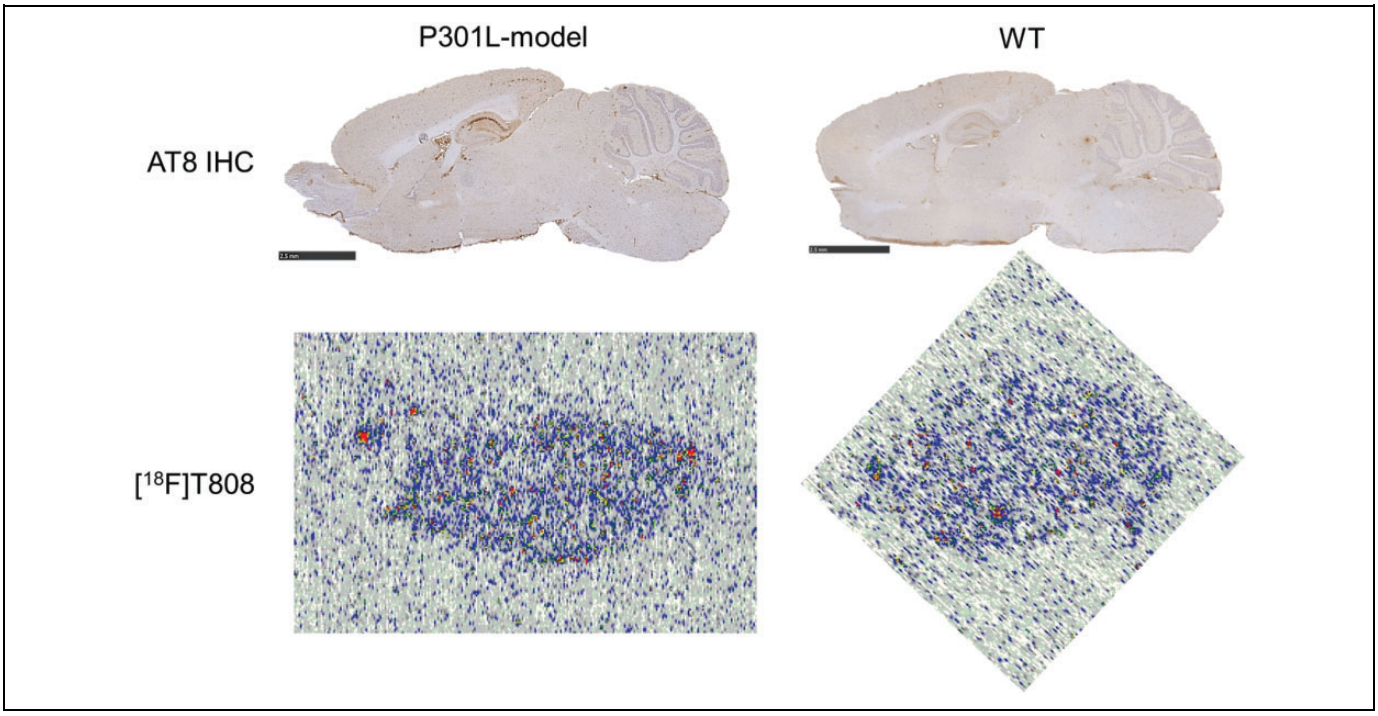

Figure 6. Autoradiography analysis on slices of the P301L-transgenic mice (left column) and their wild-type controls (right column) indicates that [^{18}F]T808 (autoradiograms on the bottom) does not specifically bind to tau tangles (microscopy images on the top, immunostained with antibodies to tau).

Table 4. pIC_{50}/K_i Values of Reference Compounds for Purified tau and Aβ.[a]

Compound	pIC_{50} – Tau	K_i – Tau	pIC_{50} – Aβ	K_i – Tau
T807	8.43	1.10	6.25	247.30
T808	7.63	9.40	<5	>4398
Lansoprazole	<5	>3998	<5	>4398
Astemizole	<5	>3998	<5	>4398
PiB	6.49	129.40	8.10	3.50
THK5105	7.07	34.00	7.27	26.60
TAU1	<5	>3998	<5	>4398
TAU4	<5	>3998	<5	>4398
TAU5	<5	>3998	<5	>4398
TAU6	<5	>3998	<5	>4398
TAU7	7.46	14.00	7.95	4.90
TAU8	<5	>3998	<5	>4398

Abbreviation: Aβ, amyloid β.
[a] pIC_{50}-values were determined from displacement curves of at least two independent experiments.

than the displacement of [^{18}F]T807 by T808. SD values of three different experiments with [^{18}F]T807, displaced by T808, showed however some variability (see Table 3). Self-block, on the other hand, was comparable for both compounds (group 1 in Table 3). Competition blocking studies showed however higher pIC_{50} values of T808 than T807 for purified tau but higher specificity of T808 compared to T807. These results are in disagreement with the published affinity values of T807 and T808. Be that as it may, Kd affinity values were determined on human AD slices in the literature, while in our competition blocking studies, purified human tau was used.[8,11] Both tracers may, however, be considered as benchmark compounds for tau, as they have high affinity and selectivity for tau fibrils. In the case of AD in which the concentration of tau aggregates in the human brain can be 5 to 20 times lower than that of Aβ aggregates,[7] high affinity combined with a high selectivity for tau is a prerequisite for a good tau PET imaging agent.

In the first group of reference ligands for the semiquantitative autoradiography experiments, authors of the Tohoku university described three tau imaging agents, among others[10,13]:

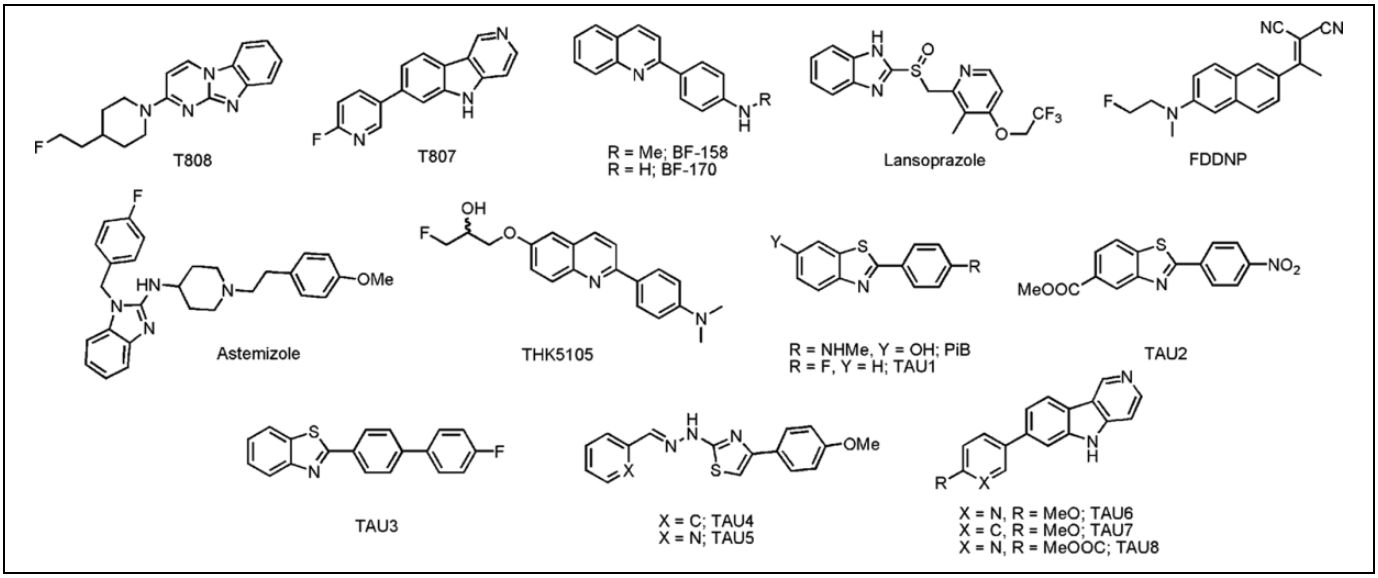

Figure 7. Chemical structures of reference compounds and newly synthesized compounds.

fluorine 18-labeled THK-5105, carbon 11-labeled BF-158, and BF-170. All of them are arylquinoline derivatives[3,13] which in our hands were able to reduce the binding of [^{18}F]T808 to NFT-rich regions in a similar range (up to 93%, see Table 3). [^{18}F]THK5105, [^{11}C]BF-158, and [^{11}C]BF-170 were all reported to have good affinities for tau (or presumed affinities as Ki values for BF-158 and BF-170 were >5000 nmol/L for Aβ fibrils). Two K_D values (a high and a low affinity site) in the nanomolar range were reported for [^{18}F]THK5105, suggesting multiple binding sites on tau fibrils.[13] The introduction of an extra methyl group on the structure of BF-170, compared to the structure of BF-158 (Figure 7), seems to lower the binding affinity for tau (respectively 84% inhibition instead of 93%) in our autoradiography assay. THK5105 was also evaluated in the competition binding assays, where it showed high affinity for tau (pIC_{50} of 7.07), but also for Aβ (pIC_{50} of 7.27), thus resulting in low selectivity. The latter results are at odds with the reported specificity of THK-5105 (25-fold specificity for tau over Aβ)[13] but could partially be explained by a different screening approach, as affinity was originally determined on recombinant $A\beta_{1-42}$ and the K18ΔK280-tau construct.[13] On the other hand, the benzimidazole compounds astemizole and lansoprazole were able to decrease binding of [^{18}F]T808 only up to 22% (see Table 3), although both imaging agents showed affinity for heparin-induced tau polymers and isolated preparations of human PHFs.[32-34] The lack of binding inhibition by both benzimidazole structures, both in autoradiography studies and in the competition binding assays, may be due to either the difference in human PHFs across the assays or the allosteric binding of astemizole and lansoprazole, compared to T808.[17]

While the arylquinoline and the benzimidazole imaging agents described earlier were only recently evaluated *in vitro* as selective tracers for tau fibrils, [^{11}C]PiB was among the first PET imaging agents developed to visualize AD pathology in the living brain.[35,36] PiB preferentially binds to senile plaques (SP).[36] As expected, PiB showed little or no inhibition of [^{18}F]T808 binding (see Table 3), confirming the fact that the binding properties of T807 and T808 are different from those of Aβ PET-imaging agents with benzothiazole scaffolds. This was confirmed by our autoradiography blocking studies in which negligible inhibition of the binding of [^{11}C]PiB was observed for T807 (11%) and T808 (17%), suggesting that these agents are relatively selective for tau versus Aβ. The latter result was also shown for T808 in the competition binding assays (Table 4).

In the second group, newly synthesized ligands were included containing scaffolds with presumed affinity for tau fibrils[8,11,37,38] such as benzothiazoles (TAU1-3), carbazoles (TAU6-8), and phenylthiazolylhydrazides (TAU4-5). Five of eight compounds tested (TAU1 and TAU5-8) were able to inhibit the binding of [^{18}F]T808 with more than 50%, three of which even displaced it more than 90%. The efficacy of the latter three compounds (TAU6-8) was expected, as they are structurally related to T807 and T808. The high potency of TAU6-8 proves that the pyridine moiety of T807 allows diverse substitution without compromising its affinity for PHFs. The absence of displacement of [^{11}C]PiB binding by these three compounds suggests that they also selectively bind to tau (see Table 3). A distinct difference was observed between TAU4 and TAU5. The latter differs from TAU4 by the presence of a pyridine ring instead of a phenyl ring, resulting in an extra 26% inhibition (see Table 3). A side chain with a pyridine ring thus might be beneficial to interact with NFTs at similar sites as T807 and T808. The ligands TAU1-3 and PiB share a similar phenyl-benzothiazole core structure, but only TAU1 inhibited [^{18}F]T808 binding to an extent of 75% (see Table 3). In the

competition binding assay, only TAU7 showed affinity for tau and Aβ (with a pIC_{50} of 7.07 and 7.27, respectively). Discrepancy between the autoradiography blocking studies and the competition binding assays could however, as previously mentioned, be explained by the fact that in the competition assays purified tau and Aβ has been used, while in the autoradiography studies both aggregated proteins are in their ''natural'' environment, as brain slices of the latest Braak stage were used.

[^{18}F]T808 was additionally evaluated in tau overexpressing transgenic mice (P301L model). We did not observe any specific binding, in contrast to the experiments using human brain slices. This may be explained by several contributing factors: differences in posttranslational modifications between mice and humans, different composition of tau-isoforms (mice only express 4R isoforms of tau, whereas 3R and 4R are equally expressed in [AD] humans). and ultrastructural differences in cross-beta sheets.[39] Similar μPET results were observed by Xia et al in the P301L transgenic mice model.[11] Nonetheless, several tau tracers (THK-523, N-methyl lansoprazole, and PBB3) were reported to bind to tau in transgenic mice models in autoradiography ARX- and μPET studies.[10,12,14] Thus, the difference in binding affinity of T808 between murine and human tau could also be explained by the fact that NFTs and SPs are subject to an aging process throughout the disease so that the structure of relatively young plaques in mouse models may be quite different from that of the older NFTs and SPs in patients with AD.[35] Hence, tau tracers may show affinity for specific subfractions of human aggregated tau, as it is the case for [^{11}C]PBB3, which is able to bind to different tau fractions (3R and/or 4R), namely, tau present not only in AD but also in other tauopathies,[14] properties which make the development of a more stable and ^{18}F-labeled compound worth pursuing.

Conclusion

By performing parallel biodistribution, metabolite, and autoradiography studies with [^{18}F]T807 and [^{18}F]T808, we were able to provide a straightforward comparison of both radioligands and establish them as benchmark compounds for *in vitro* evaluation and comparison of recently reported tau tracers and newly synthesized ligands in semiquantitative autoradiography studies. Apart from T807, only THK5105, BF-158, and BF-170 were able to displace [^{18}F]T808 up to 93%, implying affinity to similar regions as T808 (and T807). Astemizole and lansoprazole, on the other hand, show possible allosteric binding compared to T808 and T807, since their displacement of [^{18}F]T808 was negligible. In the group of newly synthesized ligands, bearing scaffolds with known affinity for tau fibrils, three derivatives of T807 (TAU6-8) showed high blocking of [^{18}F]T808. Absence of displacement of [^{11}C]PiB by these three compounds suggests that these compounds also selectively bind to tau. No specific binding of [^{18}F]T808 to murine tau in the P301L transgenic mouse model was observed. Differences in affinity between human and murine tau might be explained by interspecies differences between tau fibrils but is more likely due to existence of specific subfractions of human aggregated tau, compared to murine tau. Currently, reasonably good tau markers for AD have been developed in terms of affinity, biodistribution, and selectivity, but development of novel ligands that can target tau aggregates more selectively in different tauopathies, with little or no interaction with Aβ, and that are also able to bind to different tauopathies and transgenic mice models are required.

Acknowledgments

We thank Julie Cornelis (Laboratory for Radiopharmacy, KU Leuven) for her skillful help with the animal experiments.

Declaration of Conflicting Interests

The author(s) declared no potential conflicts of interest with respect to the research, authorship, and/or publication of this article.

Funding

The author(s) disclosed receipt of the following financial support for the research, authorship, and/or publication of this article: This research was funded by Janssen Research and Development (Beerse, Belgium)

References

1. Masters CL, Cappai R, Barnham KJ, et al. Molecular mechanisms for Alzheimer's disease: implications for neuroimaging and therapeutics. *J Neurochem*. 2006;97(6):1700-1725.
2. Hyman BT, Phelps CH, Beach TG, et al. National Institute on Aging-Alzheimer's Association guidelines for the neuropathologic assessment of Alzheimer's disease. *Alzheimers Dement*. 2012;8(1): 1-13.
3. Okamura N, Suemoto T, Furumoto S, et al. Quinoline and benzimidazole derivatives: candidate probes for in vivo Imaging of tau pathology in Alzheimer's disease. *J Neurosci*. 2005;25(47): 10857-10862.
4. Yang L, Rieves D, Ganley C. Brain amyloid imaging–FDA approval of florbetapir F18 injection. *N Engl J Med*. 2012; 367(10):885-887.
5. Gomez-Isla T, Hollister R, West H, et al. Neuronal loss correlates with but exceeds neurofibrillary tangles in Alzheimer's disease. *Ann Neurol*. 1997;41(1):17-24.
6. Arriagada PV, Growdon JH, Hedley-Whyte ET, Hyman BT. Neurofibrillary tangles but not senile plaques parallel duration and severity of Alzheimer's disease. *Neurology*. 1992;42(3 pt 1):631-639.
7. Villemagne VL, Furumoto S, Fodero-Tavoletti M, et al. The challenges of tau imaging. *Future Neurol*. 2012;7(4):409-421.
8. Zhang W, Arteaga J, Cashion DK, et al. A highly selective and specific PET tracer for imaging of tau pathologies. *J Alzheimer's Dis*. 2012;31(3):601-612.
9. Spillantini MG, Goedert M. Tau pathology and neurodegeneration. *Lancet Neurol*. 2013;12(6):609-622.
10. Fodero-Tavoletti MT, Okamura N, Furumoto S, et al. 18F-THK523: a novel in vivo tau imaging ligand for Alzheimer's disease. *Brain*. 2011;134(pt 4):1089-1100.
11. Xia CF, Arteaga J, Chen G, et al. [(18)F]T807, a novel tau positron emission tomography imaging agent for Alzheimer's disease. *Alzheimers Dement*. 2013;9(6):666-676.

12. Xia S, Garrett MC, Timothy JD, et al. Evaluation of [11C]N-methyl lansoprazole as a radiopharmaceutical for PET imaging of tau neurofibrillary tangles. *ACS Med Chem Lett*. 2013;3(11):936-941.
13. Okamura N, Furumoto S, Harada R, et al. Novel 18F-labeled arylquinoline derivatives for noninvasive imaging of tau pathology in Alzheimer disease. *J Nucl Med*. 2013;54(8):1-8.
14. Maruyama M, Shimada H, Suhara T, et al. Imaging of tau pathology in a tauopathy mouse model and in Alzheimer patients compared to normal controls. *Neuron*. 2013;79(6):1094-1108.
15. Shah M, Catafau AM. Molecular imaging insights into neurodegeneration: focus on tau PET radiotracers. *J Nucl Med*. 2014; 55(6):871-874.
16. Villemagne VL, Fodero-Tavoletti MT, Masters CL, Rowe CC. Tau imaging: early progress and future directions. *Lancet Neurol*. 2015;14(1):114-124.
17. Ariza M, Kolb HC, Moechars D, et al. Tau PET imaging: past, present and future. *J Med Chem*. 2015;58(11):4365-4382.
18. Chien DT, Bahri S, Szardenings AK, et al. Early clinical PET imaging results with the novel PHF-tau radioligand [F-18]-T807. *J Alzheimer's Dis*. 2012;34(2):457-468.
19. Chien DT, Szardenings AK, Bahri S, et al. Early clinical PET imaging results with the novel PHF-tau radioligand [F18]-T808. *J Alzheimer's Dis*. 2013;38(1):171-184.
20. Zimmer ER, Leuzy A, Bhat V, Gauthier S, Rosa-Neto P. In vivo tracking of tau pathology using positron emission tomography (PET) molecular imaging in small animals. *Transl Neurodegener*. 2014;3(1):6.
21. Szardenings AK, Kolb HC, Walsh JC, et al. Imaging agents for detecting neurological dysfunction. US patent 20120302755 Al 2012.
22. Szardenings AK, Zhang W, Kolb HC, et al. Imaging agents for detecting neurological disorders. US patent 2011/0182812 A1 2011.
23. Serdons K, Verduyckt T, Vanderghinste D, et al. Synthesis of 18F-labelled 2-(4'-fluorophenyl)-1,3-benzothiazole and evaluation as amyloid imaging agent in comparison with [11C]PIB. *Bioorg Med Chem Lett*. 2009;19(3):602-605.
24. Prabhu PP, Shastry CS, Pande SS, et al. Design, synthesis, characterization and biological evaluationof Benzothiazole-6-carboxylate derivatives. *Res Pharm*. 2011;1(2):6-12.
25. Chimenti F, Bizzarri B, Bolasco A, et al. Synthesis and biological evaluation of novel 2,4-disubstituted-1,3-thiazoles as anti-Candida spp. agents. *Eur J Med Chem*. 2011;46(1):378-382.
26. Li H, Wang C, Huang H, et al. Silver-catalyzed cascade reaction of o-aminoaryl compounds with alkynes: an aniline mediated synthesis of 2-substituted quinolines. *Tetrahedron Lett*. 2011; 52(10):1108-1111.
27. Wilson AA, Garcia A, Chestakova A, et al. A rapid one-step radiosynthesis of the *b*-amyloid imaging radiotracer N-methyl-[11C]2-(40-methylaminophenyl)-6-hydroxybenzothiazole ([11C]-6-OH-BTA-1). *J Labelled Compd Radiopharm*. 2004; 47(10):679-682.
28. Greenberg SG, Davies P. A preparation of Alzheimer paired helical filaments that displays distinct tau proteins by polyacrylamide gel electrophoresis. *Proc Natl Acad Sci U S A*. 1990;87(15): 5827-5831.
29. Pike VW. PET radiotracers: crossing the blood-brain barrier and surviving metabolism. *Trends Pharmacol Sci*. 2009;30(8): 431-440.
30. Braak H, Braak E. Neuropathological stageing of Alzheimer-related changes. *Acta Neuropathol*. 1991;82(4):239-259.
31. Marquie M, Normandin MD, Vanderburg CR, et al. Validating novel tau PET tracer [F-18]-AV-1451 (T807) on postmortem brain tissue. *Ann Neurol*. 2015;78(5):787-800.
32. Rojo LE, Alzate-Morales J, Saavedra IN, et al. Selective interaction of lansoprazole and astemizole with tau polymers: potential new clinical use in diagnosis of Alzheimer's disease. *J Alzheimer's Dis*. 2010;19(2):573-589.
33. Fawaz MV, Brooks AF, Rodnick ME, et al. High affinity radiopharmaceuticals based upon lansoprazole for PET imaging of aggregated tau in Alzheimer's disease and progressive supranuclear palsy: synthesis, preclinical evaluation, and lead selection. *ACS Chem Neurosci*. 2014;5(8):718-730.
34. Riss PJ, Brichard L, Ferrari V, et al. Radiosynthesis and characterization of astemizole derivatives as lead compounds toward PET imaging of t-pathology. *Med Chem Commun*. 2013;4(5): 852-855.
35. Shoghi-Jadid K, Small GW, Agdeppa ED, et al. Localization of neurofibrillary tangles and beta-amyloid plaques in the brains of living patients with Alzheimer disease. *Am J Geriatr Psychiatry*. 2002;10(1):24-35.
36. Klunk WE, Engler H, Nordberg A, et al. Imaging brain amyloid in Alzheimer's disease with Pittsburgh Compound-B. *Ann Neurol*. 2004;55(3):306-319.
37. Bulic B, Pickhardt M, Schmidt B. Development of tau aggregation inhibitors for Alzheimer's disease. *Angew Chem Int Ed Engl*. 2009;48(10):1740-1752.
38. Jensen JR, Cisek K, Honson NS, Kuret J. Ligand polarizability contributes to tau fibril binding affinity. *Bioorg Med Chem*. 2011; 19(17):5147-5154.
39. Duyckaerts C, Potier MC, Delatour B. Alzheimer disease models and human neuropathology: similarities and differences. *Acta Neuropathol*. 2008;115(1):5-38.